Production Engineering (2019) 13:409–424
https://doi.org/10.1007/s11740-019-00888-1

PRODUCTION PROCESS

Induction-based joining of titanium with thermoplastics

Creation and examination of titanium-thermoplastic connections

Florian P. Lugauer[1] · Andreas Kandler[1] · Stefan P. Meyer[1] · Christoph Wunderling[1] · Michael F. Zaeh[1]

Received: 20 August 2018 / Accepted: 28 January 2019 / Published online: 14 February 2019
© The Author(s) 2019

Abstract
The importance of hybrid composites is increasing, particularly with regard to structural lightweight construction. Therefore, a joining process for the production of hybrid bonds using induction technology is examined in this paper. An appropriate test rig was developed, assembled, commissioned and characterized for this purpose. Heating tests with titanium Ti6Al4V were carried out with this device to determine the influence of the process parameters on the temperature level and the temperature field. This applies in particular to the feed rate, the sample geometry, the relative positioning between sample and inductor as well as to the inductor setting like induction frequency and pulse width modulation. Based on the results of these examinations, a two-stage heating process was developed, which allows the formation of a homogeneous temperature field in the range of the melting and degradation temperature of the used polymer (PPS; Ten-Cate Cetex TC1100) and thus to achieve optimized bond strengths. More specifically, a short phase with a high energy input was used for quick and intensive warming and a longer time period was deployed to reach an even distribution of temperature. Subsequently, joints with CFRP were produced with a specimen geometry suitable for tensile shear tests according to DIN EN 1465 (Adhesives—determination of tensile lap-shear strength of bonded assemblies; German version EN 1465:2009, 2009). The analysis of the tensile shear strength and the fractured surfaces shows that the metal is much more difficult to heat up due to the melting enthalpy of the plastic than preliminary tests indicated. Further tests were carried out, which revealed a threshold value for heating where the temperature was sufficiently high to achieve a complete coating of the plastic on the metal can be achieved. In summary, the investigations showed that the presented method as well as the design of the test rig is generally suitable for bonding metal to thermoplastic polymers. The influence of various parameters on heating and bond strength could be identified. Moreover a process has been established, which allows industrially useful bonding forces. This not only proves that further investigations are useful, but also laid the foundation for further experiments.

Keywords Induction technology · Dissimilar materials · Hybrid joining · Titanium · Thermoplastics

1 Introduction

Lightweight construction is a major concern of the transport sector in order to increase energy efficiency and reduce emissions. One approach is to use different materials as required. However, this leads to heterogeneous compounds, such as metals and fiber reinforced composites (FRC), which have to be joined.

Thermal joining is an appropriate process in this case. The advantages are short cycle times, the elimination of additional material and less fibre damage compared to conventional processes such as screwing, riveting or adhesive bonding. Recent tests on adhesive joints have also shown that laser-assisted pretreatment of the metal surface can significantly increase the strength of the joint [2, 3]. For this paper, the heat supply for thermal joining was realized by electromagnetic induction to enable a contactless and flexible joining process.

✉ Stefan P. Meyer
stefan.meyer@iwb.mw.tum.de

[1] Boltzmannstr.15, 85748 Garching, Germany

2 State of the art

This section gives a brief overview of common joining processes for hybrid compounds with a focus on FRC and metal. An essential distinction for the connection of FRC with metal are in-mold assembly (IMA) and post-mold assembly (PMA) [4]. IMA processes are characterized by the fact that both the plastic component and the connection with the metallic joining partner are produced in the same process step, like injection molding. In PMA processes, two components are manufactured separately from each other and then joined together [4].

When it comes to complex or large geometries, PMA processes, like bonding, assembling (e.g. riveting, screwing, or snap joining) or thermal joining (e.g. laser beam welding, ultrasonic welding, friction welding, or induction welding), have advantages [4, 5]. However, these processes have disadvantages in terms of the curing time [6], additional mass, or the joint strength.

One way of joining two parts without additives is thermal joining (welding). For bonds with FRC and metal, only the thermoplastic component (FRC) can be melted, which then wets the metal surface and forms a bond with it. The polymer thus forms a form-fit with the metal surface [4, 7].

This gives the welded joints a weight advantage over other processes, which use additional parts or additives. Another advantage is that during the welding process the fibers in the polymer matrix cannot be displaced or damaged [8]. Various techniques such as laser welding, friction welding, or heat transfer using heating elements, are state of the art in order to supply the energy required to melt the plastic into the joint [4].

An innovative possibility is the use of induction [9]. This offers the option to introduce the energy into the joining process without contact. Reference [9] showed a method to join PA 6 GF47 with a sand blasted 22MnB5 steel with an inductive based tool. The temperature distribution in the steel was described only simulatively.

Reference [10] joined inductively aluminum with carbon fiber reinforced PA 66. It was observed that surface pretreatment with corundum blasting or acidic pickling increases the bond strength. Furthermore, the joining pressure was identified as an important process variable [10].

Reference [11] investigated compounds of PEEK and steel. He showed, that the holding temperature, holding force, and cooling rate have an influence on the bond strength. Furthermore, it is shown that the process window is limited by the degradation temperature [11].

However, the listed studies show a discontinuous process to join metal with thermoplastics. This means that large areas cannot be joined without interruption. One approach for a continuous induction welding process is examined by Ref. [12]. Here, the potential of continuous, inductive welding could be demonstrated using the example of plastic–plastic joints.

3 Objective and approach

The aim of the work presented here was to identify a process window for the inductive joining of titanium with thermoplastics. A test rig was designed and constructed for this purpose (Sect. 4). Subsequently, a test design was developed and corresponding tests were carried out for heating titanium samples (Sect. 5) and for joining titanium with a carbon fiber reinforced polymer (CFRP) (Sect. 6). The results of the test showed the basic suitability of inductive heating for thermal joining (Sect. 7).

4 Experimental setup

4.1 Examined materials

The titanium alloy Ti6Al4V was used as a metallic joining partner due to the diverse fields of application in aerospace, marine technology and motor sports. This alloy is characterized by its low density, good ductility and high strength compared to other titanium alloys [13]. Table 1 contains selected property information for this alloy.

Table 1 Properties of Ti6Al4V according to [13]

Chemical composition		
Ti	88.005–91.00	%
Al	5.50–6.75	%
V	3.50–4.50	%
Fe	0.40	%
O	0.20	%
C	0.08	%
N	0.05	%
H	0.015	%
Typical mechanical values		
Hardness	330–390	*HV*
Tensile strength	1000	MPa
Yield strength	910	MPa
Maximum elongation	18	A5D%
Physical properties (at 20 °C)		
Elastic modulus	114	GPa
Electric resistance	1.71	$\Omega\,mm^2/m$
Coefficient of thermal expansion	8.9×10^{-6}	1/K
Thermal conductivity	7.1	W/m K
Density	4.45	g/cm^3

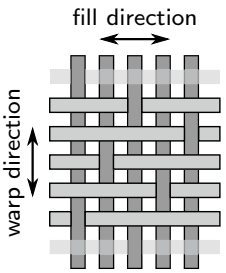

Fig. 1 Schematic drawing of the 5HS-woven fabric structure, distinguishing the warp and fill direction. The non-transparent yarns consist of the repetitive unit cells (based on [14])

Table 2 Properties of Cetex TC1100 and its matrix according to Refs. [15, 16]

Properties of the PPS-matrix		
Specific weight	1.35	g/cm^2
Glass transition temperature T_g	90	°C
Melting temperature T_m	280	°C
Decomposition temperature T_d	370	°C
Tensile strength	90.3	MPa
Elastic modulus	3800	MPa
Yield strength	3	%
Thermal conductivity	0.19	W/m K
Properties of Cetex TC1100		
Specific weight	1.55	g/cm^2
Typical processing temperature	330	°C
Tensile strength at 21 °C (0°-direction)	757	MPa
Tensile strength at 21 °C (90°-direction)	754	MPa
Elastic modulus at 21 °C (0°-direction)	55.8	MPa
Elastic modulus at 21 °C (90°-direction)	53.8	MPa

The CFRP Cetex TC1100 from TenCate Advanced Composites B.V., Nijverdal, Netherlands, consists of a semi-crystalline thermoplastic polyphenylene sulfide (PPS) matrix with a fiber to volume ratio of 50% and a fiber to weight ratio of 43%. The laminate, Carbon T300 3K 5HS 280 GSM, consists of 3000 fibres per thread in 5HS-woven fabric structure, as shown in Fig. 1, and has a grammage of 280 g/m^2. Table 2 gives an overview of the characteristics of the CFRP and its matrix material.

4.2 Requirements for the test rig

The tensile shear strength according to DIN EN 1465 has to be determined to evaluate the strength of the joint [1]. This approach is suitable considering the comparability of adhesive connections with direct thermal bonding and the fact that this test has been successfully used in several investigations [3, 11, 17]. The geometric dimensions of the specimens were determined based on this standard to a length of 100 ± 0.25 mm and a width of 25 ± 0.25 mm, with an overlap of the joining partners of 12.5 ± 0.25 mm [1]. For later industry-relevant investigations, a connection of samples with a width of up to 400 mm should be possible. To achieve a certain mechanical strength, the range of material thickness was defined to be 0.3–5.0 mm. The sample dimensions are shown in Fig. 2.

The temperature range at the surface of the metal to be achieved by induction can be derived from the thermal properties of the thermoplastic joining partner. On the one hand, the thermoplast must be heated above the melting temperature in order to achieve wetting of the metal; on the other hand, the degradation temperature must not be reached. A low viscosity is advantageous for wetting the metal surface with the plastic melt. To achieve this goal and prevent thermal degradation of the polymer, an operating point just below the degradation temperature is advantageous. Frequently used representatives of high-performance plastics with the highest operating, melting and degradation temperatures are polyether ether ether ketones (PEEK), which melt at 343 °C and decompose at 450 °C [18]. For this reason, the maximum temperature to be reached with the test rig has been set to 450 °C.

Another parameter that was specified was the operating pressure. It must be high enough to bond the surface structures of the metal completely with plastic, but on the other

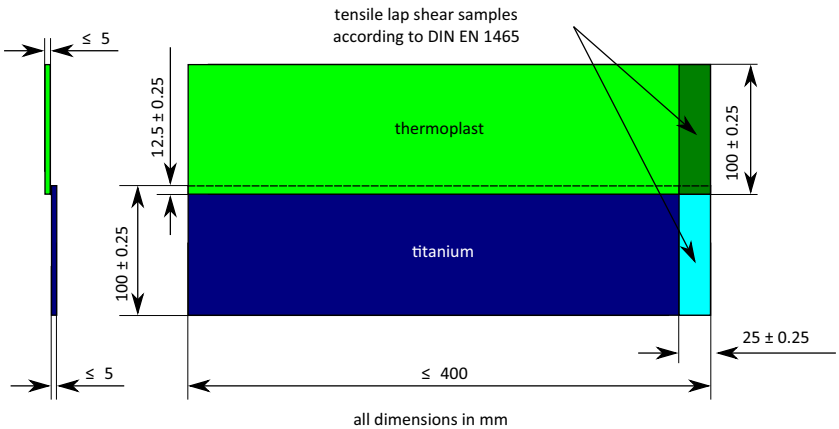

Fig. 2 Dimensions of the lap shear samples according to DIN EN 1465 [1] and maximum specimen-size

hand, the polymer must not be pressed out of the joining zone by too high pressure. Therefore, an operating pressure range of 0.1–1 bar was chosen.

4.3 Setup of the test rig

In order to fulfill the requirements mentioned in Sect. 4.2, an 'IT-0069' linear inductor in coaxial design from IFF GmbH, Ismaning, Germany, was selected for heating tests with titanium. It is controlled by a frequency generator 'EW050W' from the same company and cooled by a circulating air heat exchanger 'ProfiCool Novus PCNO-20.03-NED' from National Lab GmbH, Moelln, Germany.

The inductor was mounted on a device comprising two spindle modules of type 'SET-25-AWM-30-HK-PA-H' and 'SHTP-01-06-AWM-20-PA-HR' of IBUS GmbH, Cologne, Germany. These allow a positioning accuracy of the inductor of 0.1 mm relative to the joining zone. The remaining degrees of freedom, the assembly and the parameters d_I and p_I, which can be varied by this module, are shown in Fig. 3.

The test specimens were mounted on an single fixture with quick-release. Figure 4 gives an overview of this module. The fixture for the titanium was made of steel due to the high requirements on temperature resistance. An adjustable quick-release 'K0660.006001' from Heinrich Kipp AG, Sulz am Neckar, Germany, was attached to it. This entire part can be moved in y-direction to vary the overlap length of the specimens in the range of 2.5–22.5 mm. The holder of the thermoplastic was made of aluminum, it can be tilted via hinges and it is height-adjustable by means of screws. This allows different sample thicknesses to be compensated for and to ensure the parallelism of the joining surfaces. An additional balancing mechanism has been installed to guarantee freedom from force. To avoid distortion, the thermoplastic specimen

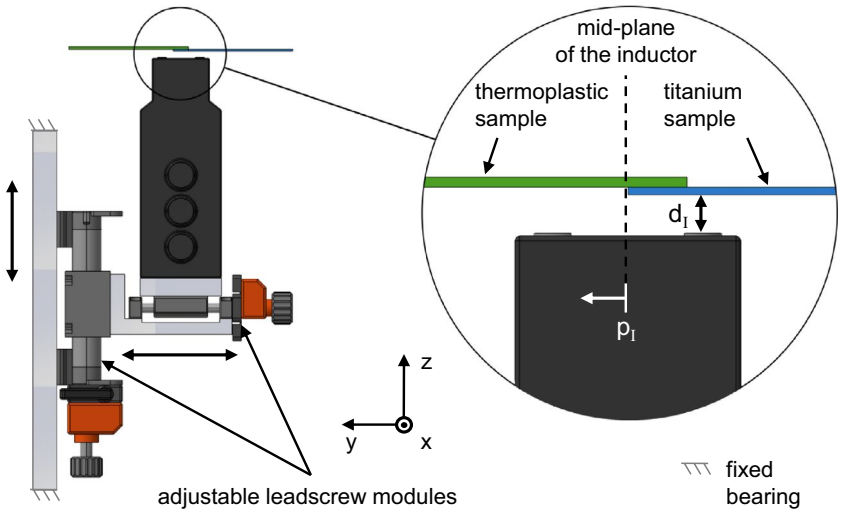

Fig. 3 Positioning of the inductor relative to the joining zone and illustration of the degrees of freedom, the displayed parameter d_I represents the distance between the top edge of the inductor's bearing surface and p_I is the distance of the inductor's mid-plane to the leading edge of the titanium sample

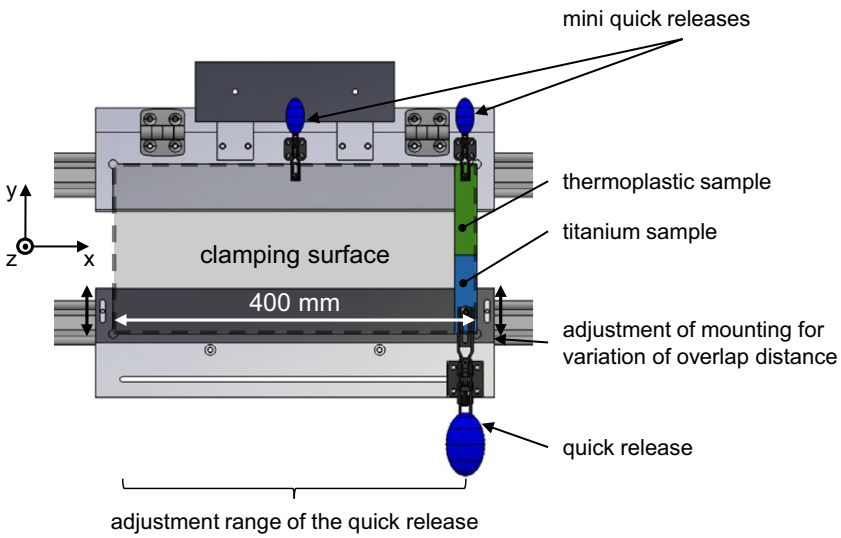

Fig. 4 Overview of the sample mountings (top view)

can be clamped down with two small quick-releases 'K0660.004001'. The assembly of the two parts to be joined is shown in Fig. 5.

To realize the feed velocity, the above-mentioned modules were mounted on two toothed belt axes 'ZLW-1040-02-B' of Igus GmbH, Cologne, with a traverse path of 1300 mm each (see Fig. 6). They are controlled by an 'EMMS-ST-57-M-SE-G2' stepper motor from Festo Vertriebs GmbH & Co. KG, Munich, Germany. To ensure synchronous movement, the motor and the axes are connected to each other via a shaft coupling. In this way, line feeds in the range of 0–2134 mm/s can be realized.

In order to apply the required joining pressure, a device was constructed consisting of two components (see Fig. 7). The upper one is designed to apply the joining force and contains a guide unit with two guide shafts 'SFUL4-38-B8-S8' from MiSUMi Europa GmbH, Schwalbach am Taunus, Germany, six pneumatic cylinders 'ADN-12-50-l-P-A-S11' from Festo Vertriebs GmbH, Esslingen-Berkheim, Germany, eight return springs 'Z-060EI' from Gutekunst+Co KG, Metzingen, Germany, and a joining head. While the add-on parts ensure clearance-free positioning of the entire upper part, the guide shafts ensure movement only in z-direction and absorb forces and moments in the other spatial directions. The pneumatic cylinders provide the necessary power transmission to the joining head.

The joining head is equipped with 17 rows of three ball bearings SS 604 ZZ 4 mm × 12 mm × 44 mm from Kugellager-Express, Schloss Holte-Stukenbrock, which touch the top of the thermoplastic and apply the joining pressure. It covers an area of 200 mm × 13 mm. The return springs have two functions: First, they pull the joining head back into its initial position in the event of an emergency stop. At the same time, they provide a preload and thus compensate for the frictional forces of the guide and the cylinders during pressure adjustment. The lower part serves as support for the metallic joining partner in order to avoid an undesirable deviation of the sample. For this purpose, a steel guide rail is supported over the joining area.

By taking into account the specified joining pressure P_j of 0.1–1 bar (see Sect. 4.2), the overlap O_j of 12.5 ± 0.25 mm according to DIN EN 1465 [1] and the width of the sample W_j of 25 mm (according to standard [1]) to 200 mm (length of the joining head) the required joining force F_j can be calculated.

With these boundary conditions the minimum force ($F_{j,min}$) and the maximum force ($F_{j,max}$) can be calculated. The results are given by Eq. 1:

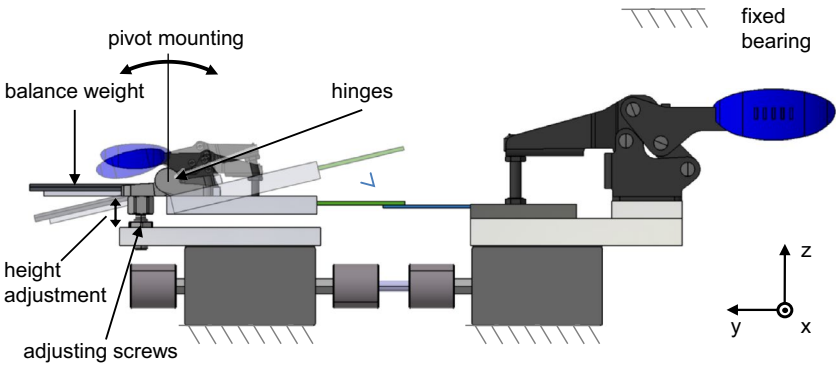

Fig. 5 Pivot mounting, height adjustment and balancing of the thermoplastic sample

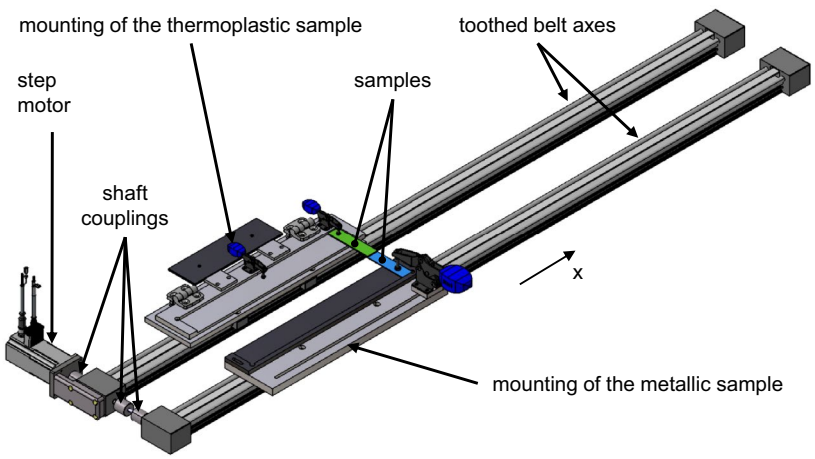

Fig. 6 Linear device consisting of step motor, shaft couplings, and toothed belt axes

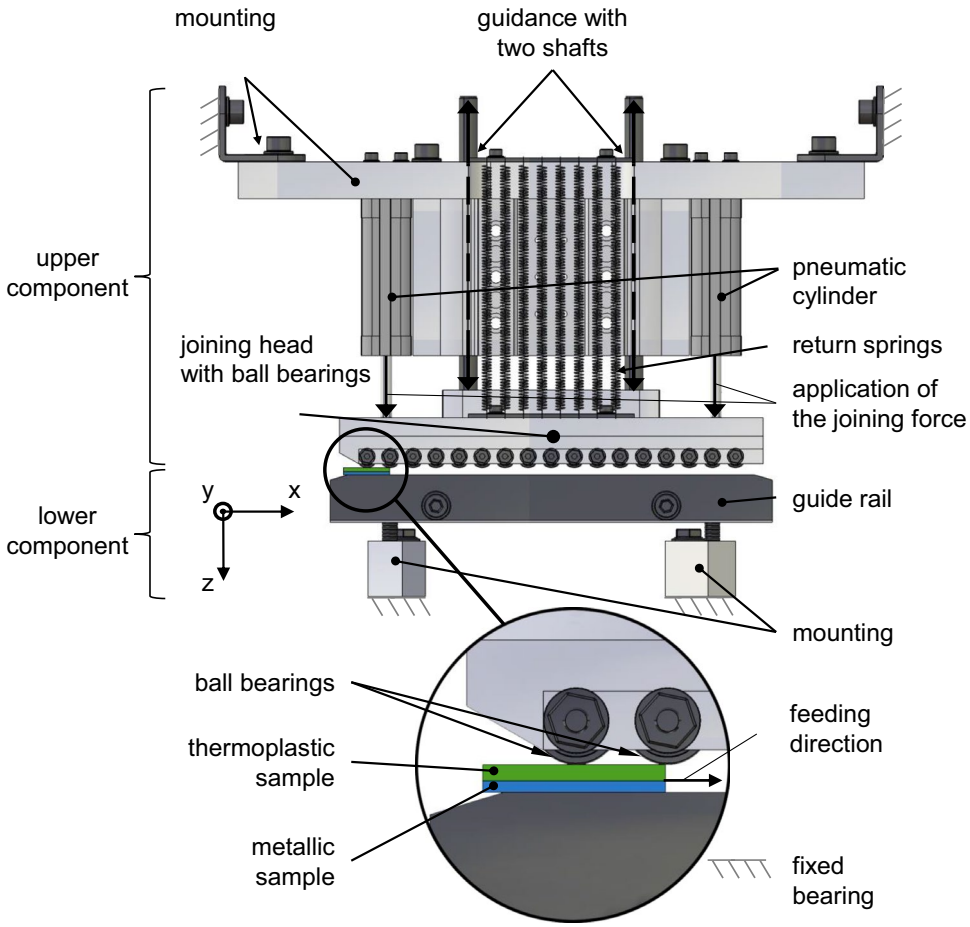

Fig. 7 Joining device to apply the joining pressure, consisting of an upper and a lower component

$$F_j = P_j \cdot O_j \cdot W_j, \tag{1}$$

$$F_{j,min} = 0.01\ \text{N/mm} \cdot 12.5\ \text{mm} \cdot 25\ \text{mm} = 3.1\ \text{N}, \tag{2}$$

$$F_{j,max} = 0.1\ \text{N/mm} \cdot 12.5\ \text{mm} \cdot 200\ \text{mm} = 250\ \text{N}. \tag{3}$$

The six pneumatic cylinders can be operated at pressures of 0.45–10.00 bar, which results in a piston force of 5.1–113.3 N. The cylinders are fitted with a pressure regulator 'VPPM-6L-L-1-G18-0L6H-V1P-S1C1' and are operated by a solenoid valve 'VUVG-L10-T32C-AZT-Q6-U-1R8RL-N5' from Festo Vertriebs GmbH. As a result, the operating pressure of all cylinders is the same and can be varied between 0.00 and 10.00 bar in steps of 0.1 bar.

To cover the specified force range and to minimize the influence of friction caused by the piston rod movements, two operational areas with two corresponding configurations of the joining unit were specified. The first one, concerning smaller joining forces between 3.1 and 87.5 N, which are relevant for specimens from 25 to 70 mm, uses only two cylinders and four return springs. In the second one, used for larger forces from 87.5 to 250 N, concerning samples of a width above 70 mm, four cylinders and eight return springs were used. These configurations were realized by plugging and unplugging of single cylinders and via mounting or demounting of the particular springs. It is important to note that the piston rods have no fixed connection to the joining head and are not moved without the aid of compressed air.

Due to the interaction of the pneumatic cylinders and the return springs, there is a linear relationship between the joining force F_j and the operating pressure P_w. This situation is visualized in the force-pressure-graph in Fig. 8. Due to the spring constant and the invariable cylinder faces, the gradient

$$m_w = \frac{F_j}{P_w} \tag{4}$$

is steady for each configuration. However, the vertical position of the curve depends on the working distance z_w. Relating to this, the upper surface of the guide rail is defined as the point of origin for the working distance z_{w0} with the associated initial joining force $F_{j,0,w0}$.

The change in the joining force F_{j,z_w} in relation to the variation of the working distance z_w can be expressed by a further gradient $k_{\Delta z_A}$:

$$k_{\Delta z_A} = \frac{\Delta F_{j,z_w}}{\Delta z_w} \tag{5}$$

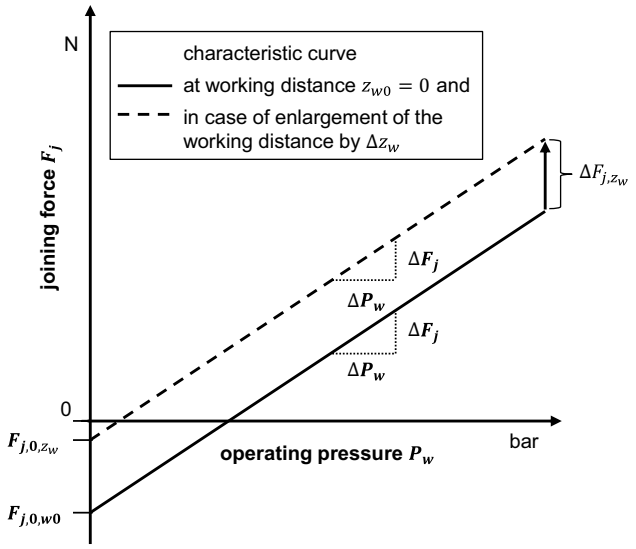

Fig. 8 Characteristic curve of the joining device regarding the influence of the working distance z_w

with

$$\Delta F_{j,z_w} = F_{j,0,z_w} - F_{j,0,w0}. \tag{6}$$

Observing the conditions mentioned above, the joining force F_j can be generally described as

$$F_j(P_w, z_w) = F_{j,0,w0} + m_w \cdot P_w + k_{\Delta z_A} \cdot z_w. \tag{7}$$

To determine the configuration-specific relationship between joining force and operating pressure, the variables of Eq. 7 had to be identified. For this purpose, the characteristic curves of each configuration were recorded at a working distance of 4.0 mm and 11.5 mm. Additionally, a regression analysis was carried out to estimate the values of $F_{j,0,w0}$ and m_w. This was done with a force sensor 'KD-40s' and the associated measuring technology of ME-Messsysteme GmbH, Henningsdorf, Germany. The results are given in Figs. 9 and 10.

On the basis of these findings, the gradient $k_{\Delta z_A}$ could be calculated by of Eq. 5. Together with an averaging of the slopes and by inserting the particular y-intercepts into Eq. 6, the joining force F_j, in dependence on the operation pressure P_w and the working distance z_w, could be estimated. The results for configuration 1 with two cylinders and four springs and for configuration 2, containing six cylinders and eight springs, are given in Eqs. 8 and 9:

$$F_{j,c1}(P_w, z_w) = -51\,\text{N} + 14\,\text{m}^2 \cdot P_w + 589\,\text{N/m} \cdot z_w, \tag{8}$$

$$F_{j,c2}(P_w, z_w) = -119\,\text{N} + 41\,\text{m}^2 \cdot P_w + 161\,\text{N/m} \cdot z_w. \tag{9}$$

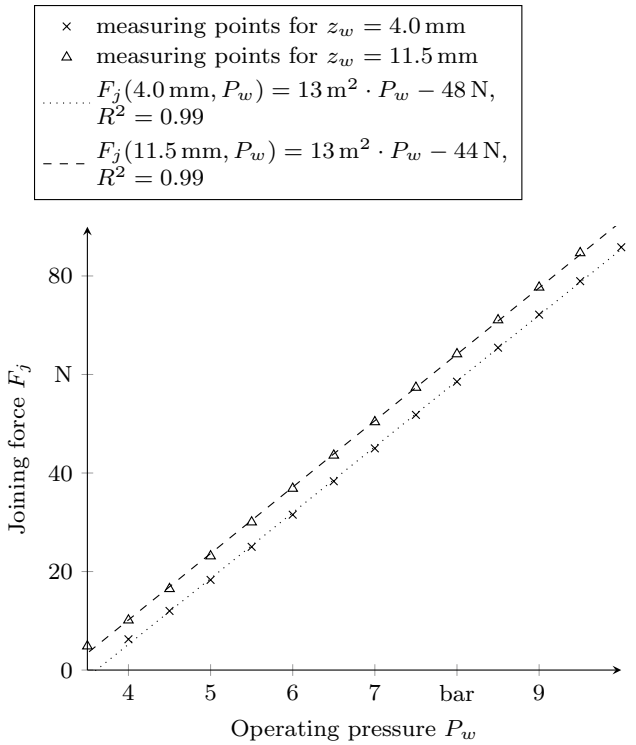

Fig. 9 Joining force F_j as a function of the operating pressure P_w for the joining device configuration with two cylinders and four springs

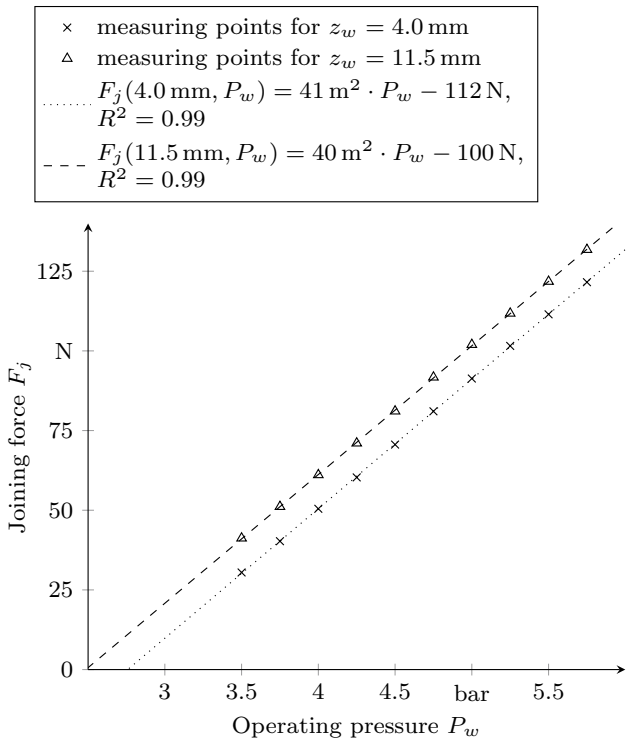

Fig. 10 Joining force F_j as a function of the operating pressure P_w for the joining device configuration with six cylinders and eight springs

For monitoring and documentation of the joining process, three infrared thermometers 'DM301 D' of the B+B Thermo-Technik GmbH, Donaueschingen, Germany, with a measurement accuracy of 1.5% were installed. They are located in the guide rail of the lower component of the joining device (cf. Fig. 7). The first one is positioned at the beginning of the rail to estimate the temperature right after the heating process, whereas the second one is in the middle of the rail. The last one measures the final temperature at the end of the guide rail. The enlargement ratio of the measuring beam is 15:1 and the initial diameter at a measuring distance of 0 mm is 7 mm. Since the sensors are located 19.0 mm beyond the metallic joining partner, the diameter at the surface is 7.19 mm and the results are averaged over an area of 40.6 mm^2.

For automation purposes, a cDAQ-Chassis '9172' of National Instruments Germany GmbH, Munich, Germany, was installed. Together with the corresponding software 'LabView 2012' and a standard desktop PC, the process parameter can be set and documented.

All above mentioned devices and units are installed in a framework made of Bosch Rexroth aluminium profiles (45 mm × 45 mm) (see Fig. 11). The frame construction is positioned on a worktable and enclosed on four sides with acrylic glass to only allow front access. To prevent hazards to people due to thermal and mechanical effects as well as by induction fields, a safety light curtain MLC510 of Leuze electronic GmbH + Co. KG, Owen, Germany was implemented. The latter shuts down the system when accessed during operation.

5 Inductive heating of titanium

As described in Sect. 4.2, it is necessary to exceed a certain temperature to bond metal and thermoplastics. For this reason, heating tests were carried out with titanium before the joining tests.

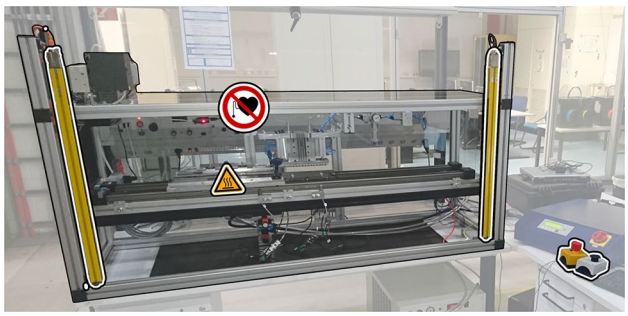

Fig. 11 Test rig for joining metal and plastics using induction. The components of the test rig are highlighted

To evaluate the heating, an infrared thermographic camera 'IR-TCM 640' from InfraTec GmbH, Dresden, Germany, with the corresponding software 'IRBIS 3 plus' was applied. In order to enable a valid measurement, the titanium specimens were pretreated with graphite spray 'GRAPHIT 33' from CRC Industries GmbH, Iffezheim, Germany, to ensure an emissivity of 0.95 [19].

For a preliminary investigation, the manufacturer's recommended settings with an induction frequency of $f_p = 20$ kHz, an induction time of $t_p = 20$ s, and a pulse width modulation value of $PMW_p = 350\,‰$ were used. The joining zone was positioned in y-direction in the center of the inductor ($p_I = 6.25$ mm, cf. Fig. 3) and at a vertical distance of $d_I = 0.5$ mm. The result is displayed in Fig. 12.

The thermographic image shows a inhomogeneous temperature distribution with two distinctive heat sources. The maximum temperature T_{max} was 398 °C, the minimum temperature $T_{min} = 241$ °C, and the average temperature $T_{avg} = 312$ °C over the joining area. This posed the following challenge: While the maximum temperature exceeded the degradation temperature $T_d = 370$ °C of the used PPS-matrix, T_{min} did not even reach the melting temperature $T_m = 280$ °C (cf. Sect. 4.1). Therefore, it was expected that a strong connection cannot be achieved in this way.

Starting from this first experiment it was necessary to investigate the influence of different process parameters

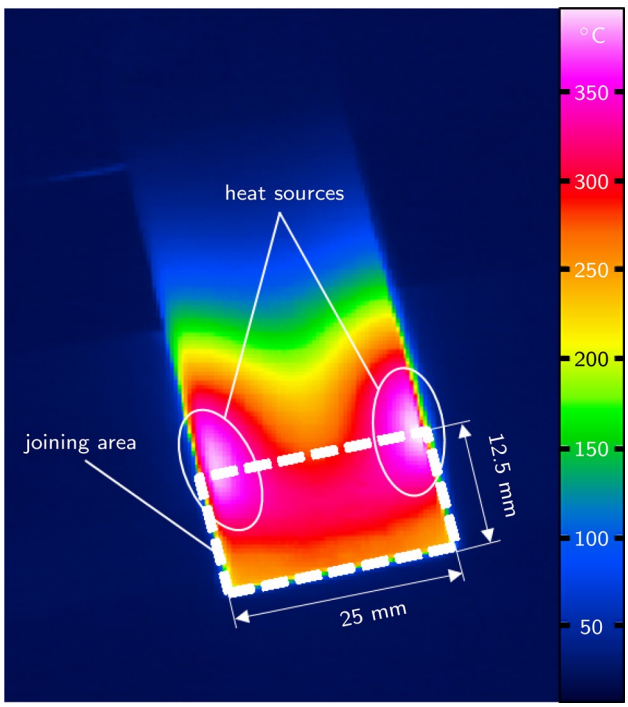

Fig. 12 Result of the first investigation with $f_p = 20$ kHz, $t_p = 20$ s, $PMW_p = 350\,‰$, $p_I = 6.25$ mm, and $d_I = 0.5$ mm

in order to realize a homogeneous temperature field in an appropriate range.

The feed rate v_p was examined within a region from 0 up to 9 mm/s in steps of 3 mm/s. Figure 13 shows an example of a static specimen in comparison to a moved specimen with the corresponding temperatures. A difference between a stationary and a moving sample in the formation of the temperature field is not recognizable. Since no influence of the feed rate could be determined, the next tests were carried out with a constant feed rate of $v_p = 3$ mm/s.

The effect of the sample width was estimated by heating the titanium with constant parameters of $f_p = 20$ kHz, $t_p = 20$ s, $PMW_p = 350\,‰$, $p_I = 3$ mm, $d_I = 0.5$ mm, and dimensions of $b = 25$ mm, 80 mm, 130 mm. The results are displayed in Fig. 14.

A direct comparison of these three cases shows that the thermal inhomogeneity is caused by the sample edges directed transversely to the inductor axis. These edges lead to a lateral displacement of the heating and to less heating of the sample corners. It can therefore be concluded that homogeneous heating is possible for large samples, but critical for small samples. On the basis of this insight, the influence of positioning can now be investigated.

The lateral sample position p_I was varied between 0 and 20 mm in steps of 2 mm to determine the formation of the temperature field by using the same parameters for the inductor and a sample with a width of $b = 25$ mm. The result after a process time of 5 s, at which the difference could be observed best, is given in Fig. 15.

The figures show correlations of the number of heat spots (in the following called heat sources), their position, and the intensity on the lateral deviation p_I. An analysis of the achieved temperature difference $\Delta T = T_{max} - T_{min}$ in the joining area indicates a minimal temperature disparity of $\Delta T = 78\,°C$ at $p_I = 16$ mm. This corresponds with the symmetrical and dense distribution of the heat sources in the corresponding thermographic image.

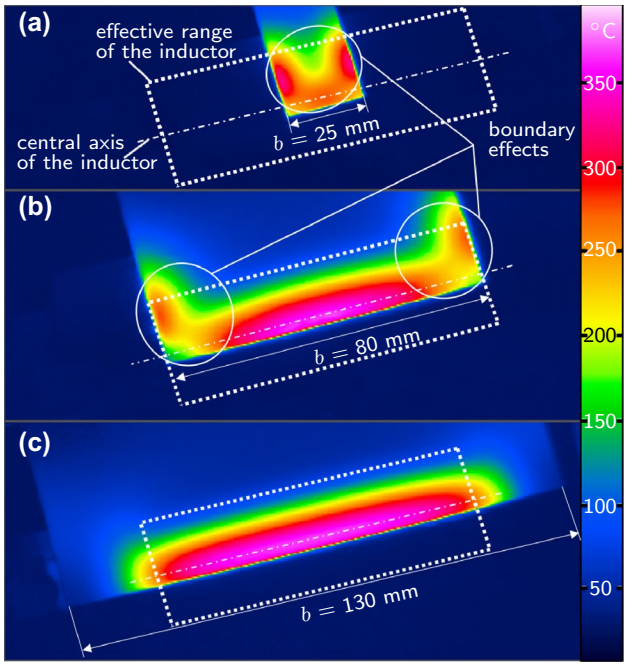

Fig. 14 Influence of the sample width on the formation of the temperature field

On the basis of these findings, the influence of the distance between inductor and sample d_I (cf. Fig. 3) was investigated at the lateral shift of $p_I = 16$ mm. The value of d_I was successively increased to 0.5 mm, 1.0 mm, 2.0 mm, 3.0 mm, 4.0 mm, 5.0 mm, 6.0 mm. The pulse width modulation PMW_p was adjusted so that T_{max} was approximately 400 °C and the results therefore comparable. Since the PMW_p has its maximum at 750 ‰, which was reached at $d_I = 4$ mm, the specified T_{max} could not be achieved at

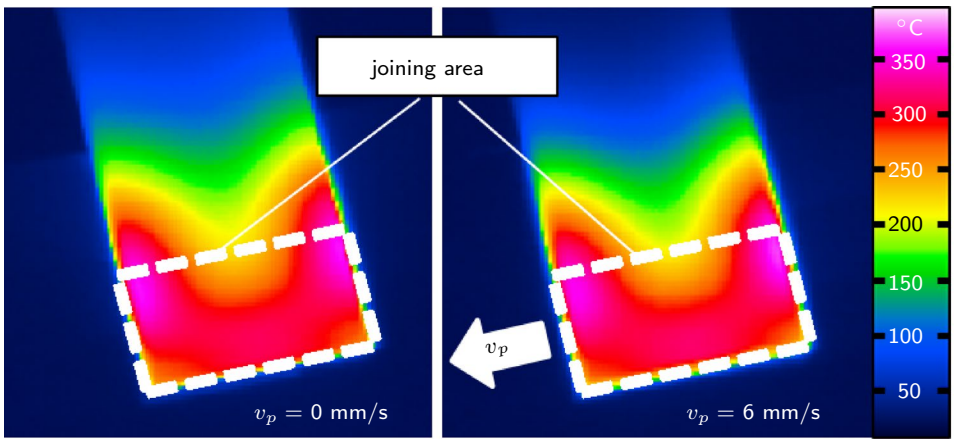

$T_{min} = 237\,°C$
$T_{avg} = 307\,°C$
$T_{max} = 364\,°C$

$T_{min} = 228\,°C$
$T_{avg} = 306\,°C$
$T_{min} = 371\,°C$

Fig. 13 Comparison of a stationary and a moved sample including the corresponding temperatures

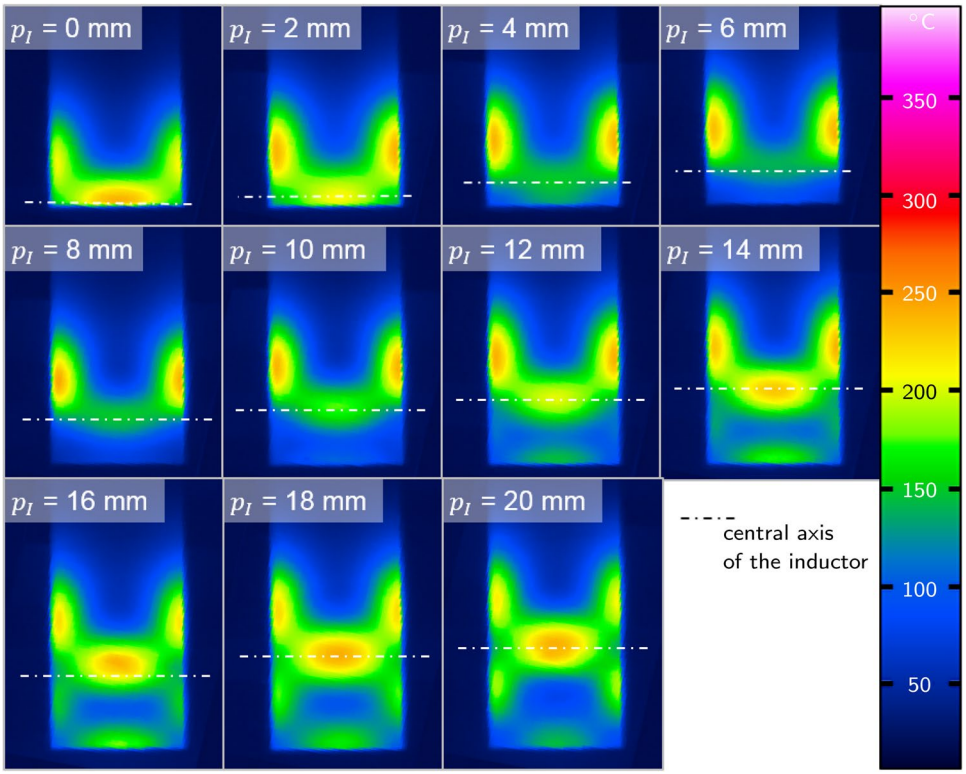

Fig. 15 Influence of the lateral shift p_I on the formation of the temperature field after 5 s of heating

distances of $d_I > 4$ mm. The other parameters were set to $f_p = 20$ kHz and $t_p = 20$ s. The results after a process time of 7 s, at which the difference could be observed best, are shown in Fig. 16.

From the necessary increase of the PWM_p value to get the same temperature, it can be concluded that the transmission efficiency decreases with increasing distance d_I. Furthermore, it can be seen that the distance Δy between the heat sources' centers and the central axis of the inductor grows with rising d_I. As a consequence of this, the temperature difference within the process zone takes the lowest value of $\Delta T = 96\,°C$ at the smallest distance $d_I = 0.5$ mm. Therefore, the smallest distance of 0.5 mm was maintained in further investigations.

The influence of the induction frequency f_p was determined by varying the value in a range between 15 and 20 kHz in steps of 2.5 kHz. The remaining parameters were set to $t_p = 20$ s, $PMW_p = 350\,‰$, $p_I = 16$ mm, and $d_I = 0.5$ mm, according to the above mentioned results. The observations after a process time of 7 s, at which the difference could be observed best, are shown in Fig. 17.

It could be shown that the warming depends on the frequency, with the strongest warming at $f_P = 15$ kHz, but is independent of the distance of the heat source and the central axis Δy. The smallest temperature difference of

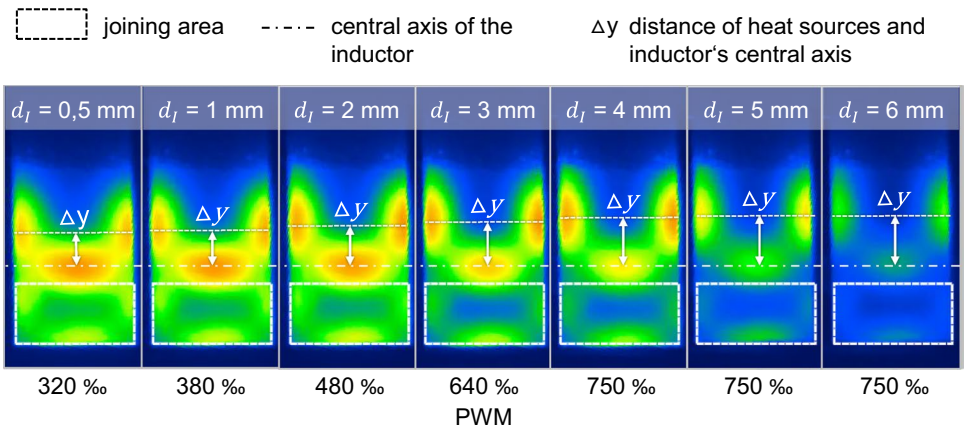

Fig. 16 Influence of the distance d_I between sample and inductor on the formation of the temperature field after 7 s of heating

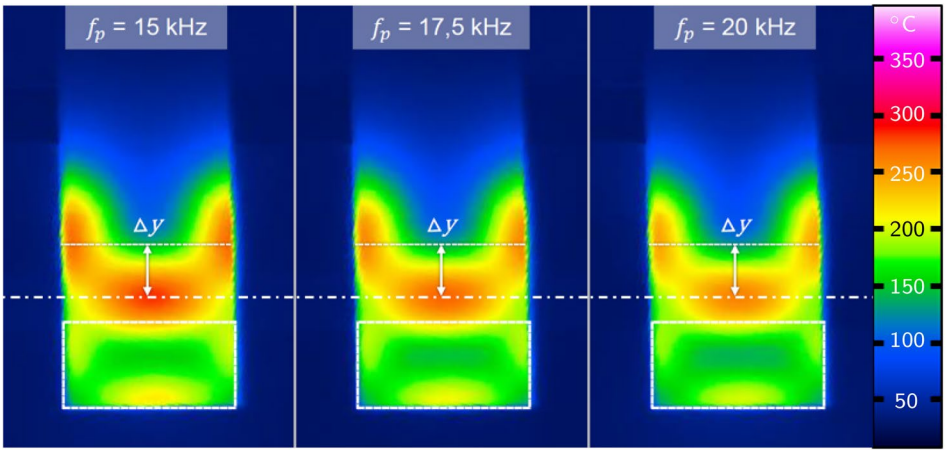

Fig. 17 Influence of the induction frequency f_p on the formation of the temperature field after 7 s of heating

$\Delta T = 109\,°C$ at the end of the process time was measured to be $f_P = 20$ kHz. Since a homogeneous heating is the main objective, along with the proper temperature range, this frequency was taken for the execution of further investigations.

In all investigations described so far, the temperature difference ΔT was larger than 78 °C. This is seen critically in the light of the specified process window from $T_m = 280\,°C$ to $T_d = 370\,°C$ [16], whereas a typical process temperature is defined to be $T_p = 330\,°C$. This means that the achieved temperature range is just below the size of the process window or exceeds the optimum process window significantly and therefore it is presumably not possible to create a stable joint connection in this way.

To meet this challenge, the process was divided into two parts: a short sequence with a high energy input for a rapid and strong heating of the material and a longer sequence with low energy input to achieve a homogenization of the temperature field. Based on the previous parametric studies, the settings presented in Table 3 have been made. The results of the corresponding experiments are displayed in Figs. 18 and 19.

As can be seen from the graphs, it is possible to comply with the specified conditions with the applied parameter settings. Both the minimum and the maximum temperature were within the desired range over a certain period and the difference between them was much smaller than the process window. Moreover, ΔT was decreasing in the course of the process. This continued until a time of $t_p = 80$ s, when the temperature difference no longer decreased. Shortly thereafter, the maximum temperature T_{max} exceeds the upper limit of the process range. As a conclusion of these findings, the further experiments were executed with an adapted process time $t_p = 70$ s, as shown in Table 4. For reasons of statistical validation, the heating experiments were repeated nine times with the adapted parameter set. While the temperatures at the end of the process are given in Fig. 20, Table 5 lists the global temperature values. Both show that all deviations are

Table 3 Parameter settings of the heating experiment with two process sequences

General process settings		
v_p	0	mm/s
b	25	mm
p_I	16	mm
d_I	0.5	mm
Inductor settings of the first process sequence		
$t_{p,1}$	3.5	s
$PWM_{p,1}$	750	‰
$f_{p,1}$	20	kHz
Inductor settings of the second process sequence		
$t_{p,2}$	176.5	s
$PMW_{p,2}$	195	‰
$f_{p,2}$	20	kHz

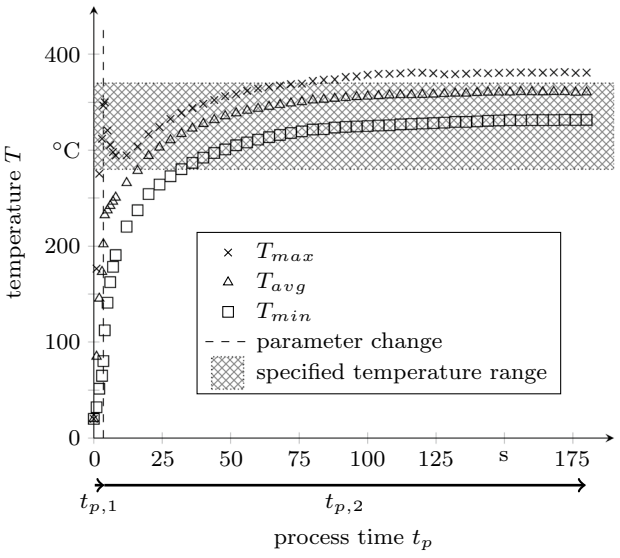

Fig. 18 Maximum temperature T_{max}, average temperature T_{avg} and minimum temperature T_{min} as a function of the process time t_p during the heating with the process parameters given in Table 3

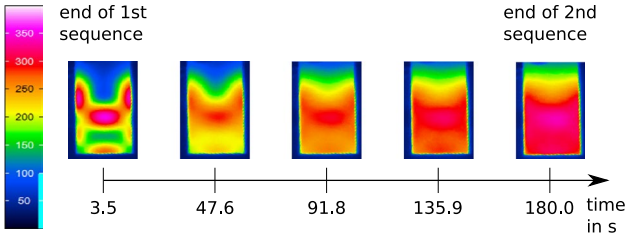

Fig. 19 Time-dependent temperature distribution in the joining zone; $t = 3.5$ s corresponds to the state after the first stage. $t = 47.6$ s to $t = 180.0$ s shows the temperature distribution during the homogenization phase

Table 4 Adapted parameter settings of the heating process with two sequences

General process settings		
v_p	0	mm/s
b	25	mm
p_I	16	mm
d_I	0.5	mm
Inductor settings of the first process sequence		
$t_{p,1}$	3.5	s
$PWM_{p,1}$	750	‰
$f_{p,1}$	20	kHz
Inductor settings of the second process sequence		
$t_{p,2}$	70.0	s
$PWM_{p,2}$	195	‰
$f_{p,2}$	20	kHz

within the specified process window. Furthermore, it can be seen that the fluctuations are below or close to the measuring accuracy of the thermal camera of 2%. It can therefore be stated that sufficient repeatability is achieved for the following joining tests.

6 Induction based joining of titanium and thermoplastics

The surfaces of the metallic joining partners were modified in order to carry out the joining tests. For this purpose, a nano-structure according to Ref. [20] was applied by the aid of a pulsed laser source 'Powerline E Air 25' from ROFIN-SINAR Laser GmbH, Hamburg, Germany. This procedure proved to be useful for the improvement of the adhesion behavior in the past. The parameters used are given in Table 6. Whereas the titanium specimens were purchased from Airbus Group, Leiden, Netherlands, the CFRP samples were delivered from the same manufacturer in plates and cut with a water jet.

To realize a joining, the joining partners have to go through the two-stage warming process described in Sect. 5.

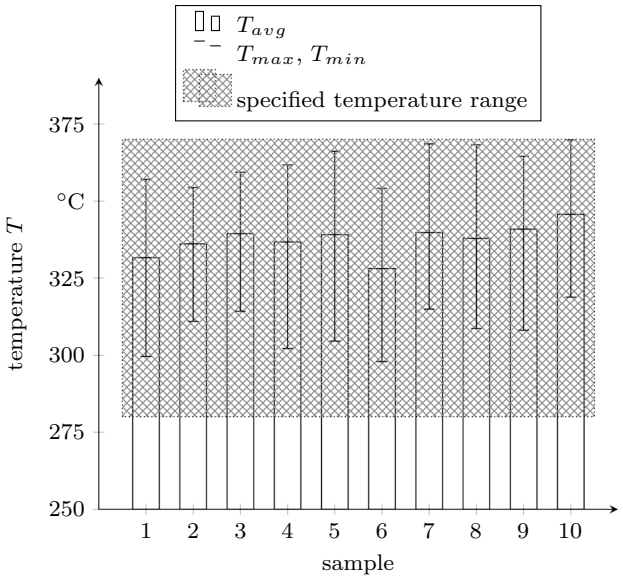

Fig. 20 Repetition of the warming experiments for the purpose of statistical validation; temperatures at the end of the process times

Table 5 Results of the statistical validation

Parameter	T_{max}	T_{avg}	T_{min}	
Maximum value	370	346	319	°C
Minimum value	354	328	298	°C
Average value	362	338	308	°C
Standard deviation	5.9	4.9	7.0	°C
Relative standard deviation	1.6	1.5	2.3	%

Table 6 Parameter settings of the laser structuring process

Parameter	Value	
Power density	0.43	GW/cm^2
Pulse duration	16.3	ns
Frequency	10	kHz
Amperage	30	A
Focal length	300	mm
Line spacing	80	µm
Number of passes	1	
Velocity	800	mm/s
Beam width	106 ± 4	µm

The specified process pressure was adjusted according to Eqs. 8 and 9 respectively and applied by using the joining device. Since the investigations of Sect. 5 showed that it takes about 65 s for the metal to cool down below the glass transition temperature of 90 °C, the feed rate for the pressure application was set to 3 mm/s. In this way, the complete strength is reached at the end of the joining process.

Table 7 Initial experimental design of the joining investigations

PMW_2 (‰)	P_J in $\frac{N}{m^2}$		
	0.4	0.6	0.8
195		E03	
193	E02	E01	E04
191		E05	

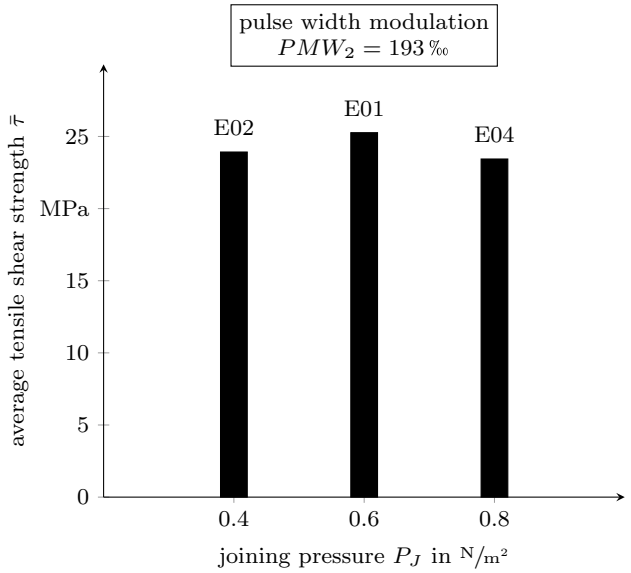

Fig. 21 Results of preliminary experiments with constant PWM_2

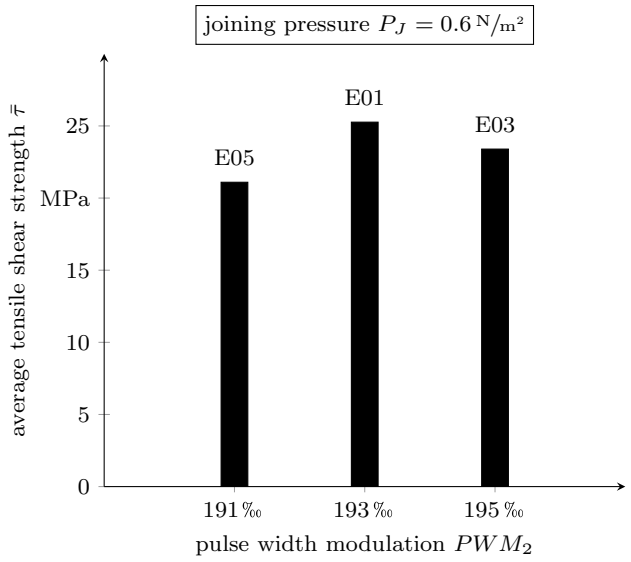

Fig. 22 Results of preliminary experiments with constant P_J

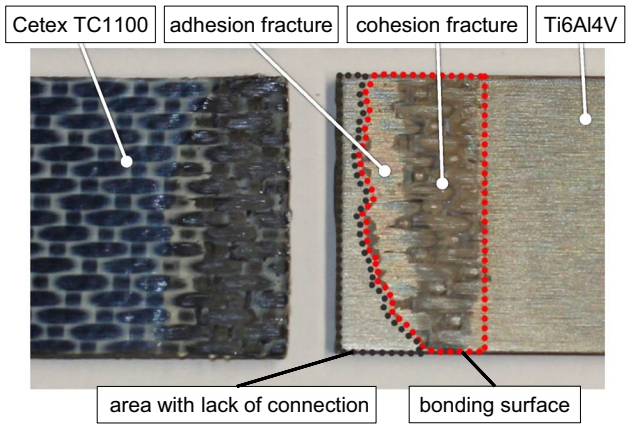

Fig. 23 Experiment E01: fracture surfaces after the tensile test with areas of cohesion and adhesion fracture as well as the section without connection

For a first exploratory study, the experimental design shown in Table 7 was used. The numbering reflects the execution order; each measurement was repeated once. The tensile shear strength τ of the compound was measured by means of a tensile/compression testing machine 'Z020' of Zwick GmbH & Co. KG, Ulm, Germany. The test procedure was force controlled and a force increase of 125 N/s was applied. The results are displayed in Figs. 21 and 22.

The data show that tensile strengths between 21.1 and 25.3 MPa could be achieved. The maximum value resulted from the combination of $P_J = 0.6\,\mathrm{N/m^2}$ and $PWM_2 = 193\,‰$. However, the optical examination of the fracture surfaces revealed that only partial bonding was accomplished. Figure 23 shows this situation: The areas of cohesion and adhesion fracture as well as a section without connection can be clearly differentiated.

The damage pattern leads to the conclusion that the necessary heating could not be achieved over the whole area, despite the use of the parameters determined in the preliminary tests. This is probably caused by the heat transfer between the joining partners and the heat conduction in the fiber composite material. Based on these results, the further procedure was designed as follows: In order to investigate the relationship between the process temperature T_p, the melting process, and the tensile shear strength τ, only the titanium sample without a plastic sample was initially heated and the temperature T_1 was measured at the end of the heating by means of the built-in pyrometer. The pyrometer position is 6 mm behind the inductor and 19 mm below the metal specimen. Subsequently, the procedure was repeated with applied CFRP sample and the temperature $\tilde{T}_1$ at the end of the process was determined. The value combinations shown in Table 8 were tested twice. The first three results were taken from the previous experiments. The joining pressure P_J was left constant at the best value of 0.6 N/m^2 of the first series of tests.

The thermal behavior of the sample bodies is shown in Fig. 24; the tensile strengths in each case as a function of the temperature are displayed in Fig. 25.

The results show an increase in temperature T_1 of titanium with an upturn in pulse width modulation PWM_2. The temperature of the material combination $\tilde{T}_1$ had a smaller increase. This leads to a rise in the difference between the two values from 32 °C at $PWM_2 = 197$ ‰ to a maximum of 57 °C at $PWM_2 = 217$ ‰, which corresponds to an enlargement of 80%. The heating was always in the specified process range, but the heat input in the thermoplastics increased considerably with increasing pulse width modulation PWM_2. This should lead to an enlarged and more extensive melting of the matrix and thus also to an improved connection.

This assumption is confirmed by a consideration of the tensile shear tests. The tensile shear strength τ shows an expansion with rising temperature $\tilde{T}_1$ and therefore with increasing temperature difference T_1–$\tilde{T}_1$. However, a significant increase only from 21.1 MPa at $PWM_2 = 191$‰ to 29.8 MPa at $PWM_2 = 201$ ‰ can be observed, which corresponds to a gain of 41.2%. As a result, the value remains stable in a range of 28.4–30.9 MPa.

This behavior can be explained by considering the failure process. As Fig. 26 shows, the bonding surface increases with increased heating until the complete area is connected at $PWM_2 = 205$ ‰.

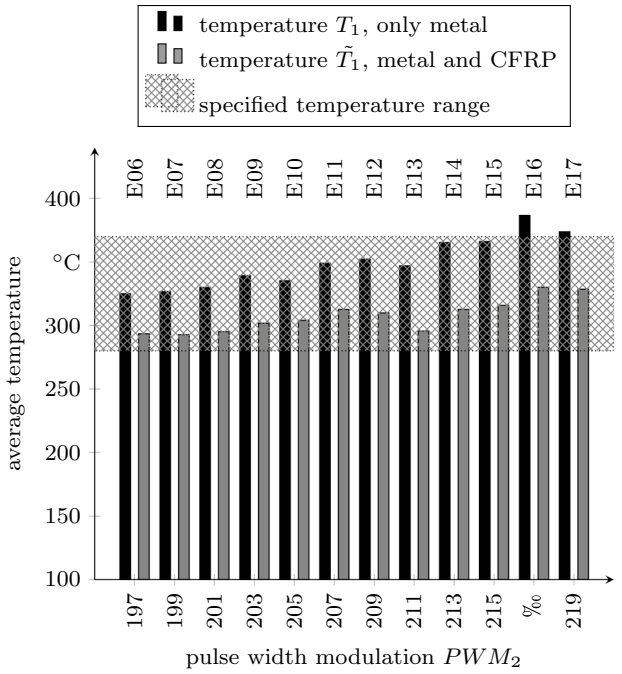

Fig. 24 Average temperatures of titanium (T_1) and titanium with CFRP ($\tilde{T}_1$) at the end of heating depending on different pulse width values PMW_2 and at constant joining pressure of 0.6 N/m^2

Table 8 Adapted experimental design of joining investigations; the first three results were taken from the previous experiments

Pulse width modulation PMW_2 in ‰	Joining pressure P_J in N/m^2
191	*E*05
193	*E*01
195	*E*03
197	*E*06
199	*E*07
201	*E*08
203	*E*09
205	*E*10
207	*E*11
209	*E*12
211	*E*13
213	*E*14
215	*E*15
217	*E*16
219	*E*17

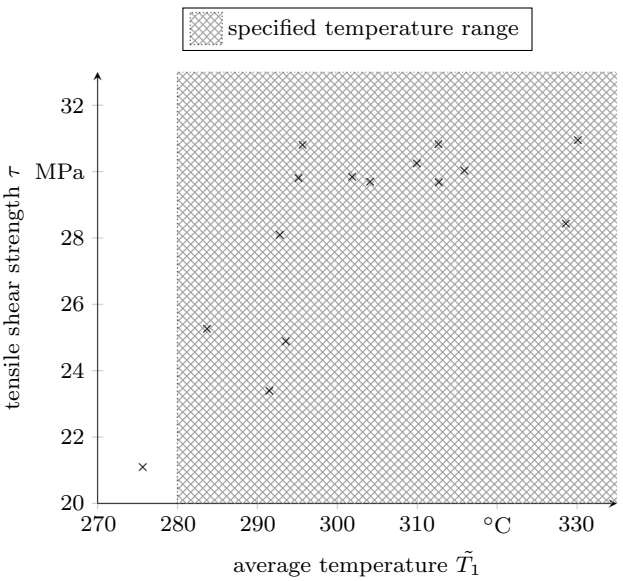

Fig. 25 Tensile shear strength τ as a function of the average temperature of titanium with CFRP ($\tilde{T}_1$) at the end of the heating phase at constant joining pressure of 0.6 N/m^2

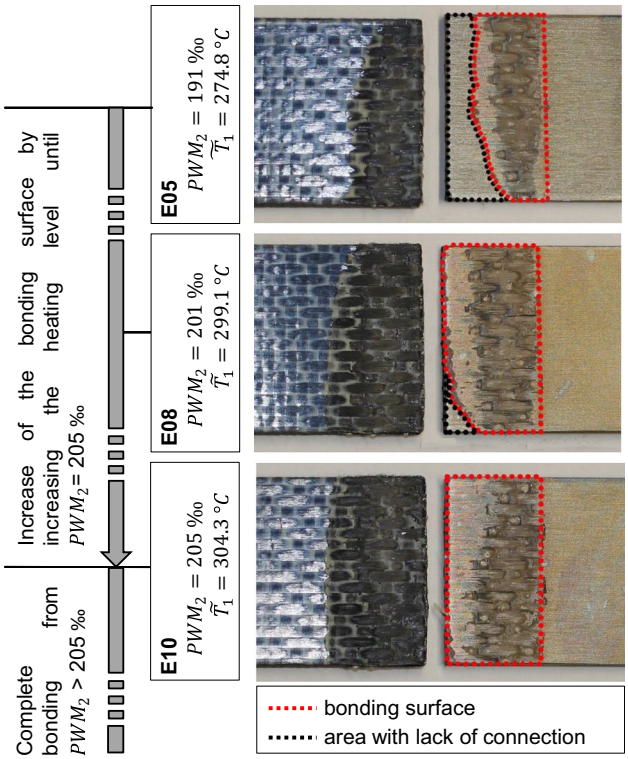

Fig. 26 Enlargement of the bonding surface until a complete connection is achieved

7 Summary and outlook

In the context of the work presented in this paper, a device for the creation of titanium-thermoplastic connections was developed and assembled. The functionality of the test rig could be proven and different heating experiments with titanium were conducted. The latter showed that a homogeneous warming of titanium within the required temperature range is possible with the chosen components by using a two-stage heating process. Furthermore, the influence of several parameters was examined.

Joining experiments were carried out based on these findings. They showed that the titanium has to be warmed up much more than originally anticipated to gain a sustainable connection. It was possible to determine a threshold value, above which a complete connection could be achieved.

In summary, the basic proof of functionality was provided and the influence of several parameters was shown. Further experiments should focus on the effect of the joining pressure. Moreover, the transferability from standardized tensile lap shear samples to other geometries should be investigated. The production and testing of actual industrial components and the transfer into practice should be the final objective.

Acknowledgements This research and development project is funded by the German Federal Ministry of Education and Research (BMBF) within the Program "Innovations for Tomorrow's Production, Services, and Work" (02P16Z002) and managed by the Project Management Agency Karlsruhe (PTKA). The author is responsible for the contents of this publication.

SPONSORED BY THE
Federal Ministry of Education and Research

OpenAccess This article is distributed under the terms of the Creative Commons Attribution 4.0 International License (http://creativecommons.org/licenses/by/4.0/), which permits unrestricted use, distribution, and reproduction in any medium, provided you give appropriate credit to the original author(s) and the source, provide a link to the Creative Commons license, and indicate if changes were made.

References

1. DIN EN 1465 (2009) Adhesives—determination of tensile lap-shear strength of bonded assemblies; German version EN 1465:2009
2. Roesner A, Scheik S, Olowinsky A, Gillner A, Reisgen U, Schleser M (2011) Laser assisted joining of plastic metal hybrids. Phys Proc 37:370–377
3. Heckert A, Zaeh MF (2014) Laser surface pre-treatment of aluminium for hybrid joints with glass fibre reinforced thermoplastics. Phys Proc 56:1171–1181
4. Reisgen U, Schleser M, Scheik S et al (2011) Novel process chains for the production of plastics/metal-hybrids, concurrent enterprising (ICE), 2011. In: 17th International conference on concurrent enterprising, electronic, Aachen **(ISBN: 978-3-943024-05-0)**
5. Ehrig F, Wey H (2007) Foil technology for metal surfaces. Kunststoffe Int 11:38–40
6. Baldan A (2003) Adhesively-bonded joints and repairs in metallic alloys, polymers and composite materials. J Mater Sci 39:1–49
7. Heckert A (2016) Gas-tight thermally joined metal-thermoplastic connections by pulsed laser surface pre-treatment. Phys Proc 83:1083–1093
8. Ageorges C, Ye L, Hou M (2001) Advances in fusion bonding techniques for joining thermoplastic matrix composites. Compos Part A Appl Sci Manuf 32:839–857
9. Kraeusel V, Froehlich A, Kroll M, Rochala P, Kimme J, Wertheim R (2018) A highly efficient hybrid inductive joining technology for metals and composites. CIRP Ann 67(1):5–8
10. Mitschang P, Velthuis R, Emrich S, Kopnarski M (2009) Induction heated joining of aluminum and carbon fibre reinforced nylon 66. J Thermoplast Compos Mater 22:767–801
11. Velthuis R (2007) Induction welding of fiber reinforced thermoplastic polymer composites to metals, Dissertation, Institut für Verbundwerkstoffe, Kaiserslautern
12. Mitschang P, Rudolf R, Neitzel M (2002) Continous induction welding process, modelling and realisation. J Thermoplast Compos Mater 15:127–153
13. Thyssenkrupp Materials Schweiz AG (2016) Titan Grade 5. http://www.thyssenkrupp.ch/documents/Titan_Grade_5.pdf. Accessed 5 Oct 2017
14. Akkerman R (2005) Laminate mechanics for balanced woven fabrics. Compos Part B Eng 37:108–116
15. TenCate Advanced Composites BV (2016) Product datasheet. https://www.tencatecomposites.com/media/221a4

fcf-6a4d-49f3-837f-9d85c3c34f74/0EEq4g/TenCate%20Advanced%20Composites/Documents/Product%20datasheets/Thermoplastic/UD%20tapes,%20prepregs%20and%20laminates/TenCate-Cetex-TC1100_PPS_PDS.pdf. Accessed 9 Oct 2017
16. Designing with fortron—polyphenylene sulfide, design manual (FN-10). http://www.hipolymers.com.ar/pdfs/fortron/diseno/Designing%20with%20Fortron%20PPS.PDF. Accessed 16 Jan 2018
17. Amend P, Mohr C, Roth S (2014) Experimental investigations of thermal joining of polyamide aluminum hybrids using a combination of mono- and polychromatic radiation. Phys Proc 56:824–834
18. Fast eine Mio. t Hochleistungskunststoffe, K-Zeitung (2014) https://www.k-zeitung.de/fast-eine-mio-t-hochleistungskunststoffe/150/1193/82119/. Accessed 28 Dec 2017
19. Fachbereich Prozessmesstechnik und Strukturanalyse (2014) Temperature measurement in industry—radiation thermometry—maintenance and intended operation of radiation thermometers, VDI/VDE 3511 Sheet 4.2, VDI/VDE-Gesellschaft Mess- und Automatisierungstechnik (ed). https://m.vdi.de/uploads/tx_vdirili/pdf/2082664.pdf
20. Kurtovic A, Brandl E, Mertens T, Maier HJ (2013) Laser induced surface nano-structuring of Ti-6Al-4V for adhesive bonding. Int J Adhes Adhes 45:112–117

Publisher's Note Springer Nature remains neutral with regard to jurisdictional claims in published maps and institutional affiliations.